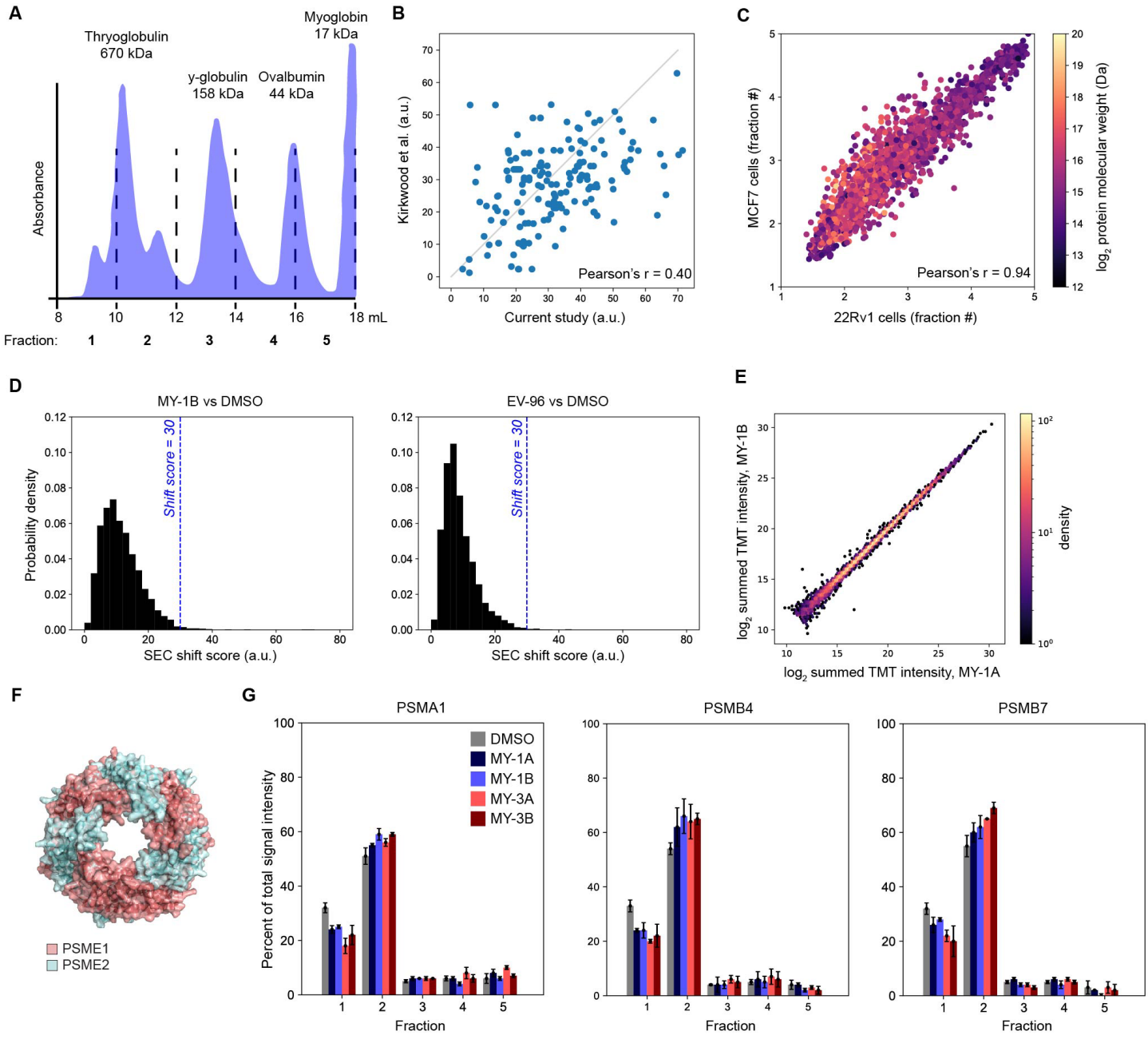

Figure S1. A proteomic platform to discover small-molecule modulators of protein-protein interactions in human cells, related to **Figure 1**.

A. Distribution of proteins of indicated MWs as fractionated by SEC-MS method.
B. Co-elution scores for protein complexes in the CORUM Core Complex dataset for both SEC-MS with 5 fractions (x-axis) and the data from Kirkwood *et. al.*[1] with 40 fractions (y-axis). Each dot represents a single annotated protein complex – lower score represents tighter co-elution of complex members. Data are mean pairwise Euclidean distance across constituent proteins in each annotated protein complex from n = 3-11

independent experiments (current study) and n = 3 independent experiments from Kirkwood *et al*.

C. Comparison of the weighted average elution times in SEC-MS experiments for proteins from 22Rv1 (x-axis) for MCF7 (y-axis) cells under control (DMSO) conditions. Each dot represents a single protein detected in both cell lines, and proteins are colored based on their annotated MW (UniProt). Large proteins elute in higher-MW fractions, while small proteins elute across all fractions, indicating the capture of native protein complexes. Data are mean elution times (weight average) of n = 2-11 and n = 2-6 independent experiments for 22Rv1 and MCF7 cells, respectively with Pearson's r indicated.
D. Distribution of SEC shift scores (a.u.) for proteins detected in MY-1B or EV-96 treated samples (20 μM, 3 h). The vertical dashed line marks a size shift value of 30, which was used as a minimal shift magnitude to designate potential compound-induced changes of interest. Data are shift scores calculated from average protein elution profiles from n = 2-11 independent experiments.
E. Comparison of protein abundances in MY-1A vs MY-1B-treated 22Rv1 cells. Data are $\log_2$ transformed summed TMT intensities for proteins quantified from cells treated with MY-1A (TMT channels 1 – 5) or MY-1B (channels 6 – 10). Data for a total of 6395 unique quantified proteins is shown. Individual values from n = 2 independent experiments are shown.
F. Structure of PA28 complex, showing heteroheptameric arrangement of PSME1 and PSME2 subunits (PDB 7DRW).
G. SEC elution profiles for representative 20S core proteasome subunits, revealing that these proteins are not size-shifted by MY-1B or other stereoisomeric azetidine acrylamides (20 μM, 3 h). Data are average values ± SEM of the fractional distribution of protein reporter ion intensities from n = 2-11 independent experiments.

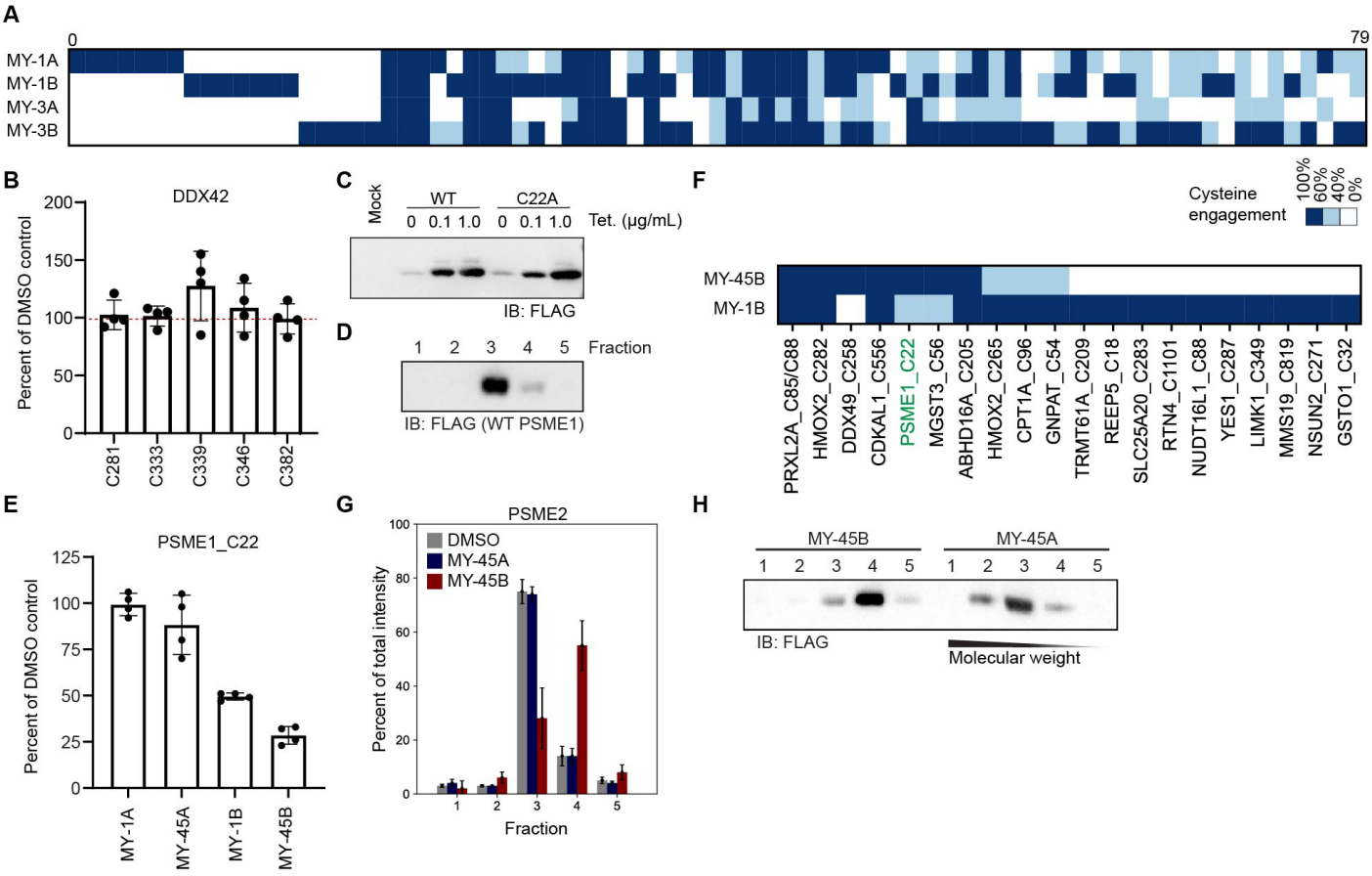

Figure S2. Electrophilic compounds stereoselectively disrupt the structure of the PA28 complex by engaging C22 of PSME1, Related to **Figures 2** and **3**.

A. Heatmap of cysteines liganded (> 60% engagement) by azetidine acrylamides in 22Rv1 cells (20 μM compound, 1 h). Data are average values from n = 4 independent experiments.

B. Lack of engagement of cysteines in DDX42 by EV-96 as measured by cysteine-directed ABPP experiments performed in 22Rv1 cells (20 μM EV-96, 1 h). Data are average values ± SD relative to DMSO from n = 4 independent experiments.

C. Western blot of 22Rv1 TetR cells expressing recombinant FLAG epitope-tagged WT- or C22A-PSME1 (10 cm dish, 1 μg plasmid, 48 h transfection) in response to treatment with the indicated amounts of tetracycline (Tet). 0.1 μg/mL of Tet was selected as the concentration for inducing expression of PSME1 protein in 22Rv1 TetR cells. 22Rv1 cells stably expressed a Tet repressor and were transiently transfected with a plasmid containing PSME1 cDNA under control of a Tet operator/CMV promoter.

D. SEC elution profile as determined by western blotting for recombinant WT-PSME1 in 22Rv1 TetR cells. Data are from a single experiment representative of two independent experiments.

E. Quantification of PSME1_C22 engagement by the indicated compounds as measured by cysteine-directed ABPP performed in 22Rv1 cells (5 μM compound, 3 h). Data are average values ± SD relative to DMSO from n = 4 independent experiments.

F. Heatmap of cysteines liganded by MY-1B or MY-45B (5 μM, 3 h) in 22Rv1 cells as determined by cysteine-directed ABPP. A cysteine was considered liganded if it showed a > 60% reduction in IA-DTB labeling in compound-treated cells. Data are average values from n = 4 independent experiments.
G. SEC-MS elution profile for endogenous PSME2 in 22Rv1 cells treated with DMSO, MY-45A, or MY-45B (20 μM, 3 h). Data are average values ± SEM of the fractional distribution of reporter ion intensities from n = 2-11 independent experiments.
H. SEC elution profile as determined by western blotting recombinant WT-PSME1 in 22Rv1 TetR cells treated with MY-45A or MY-45B (5 μM, 3 h). Data are from a single experiment representative of 2 independent experiments.

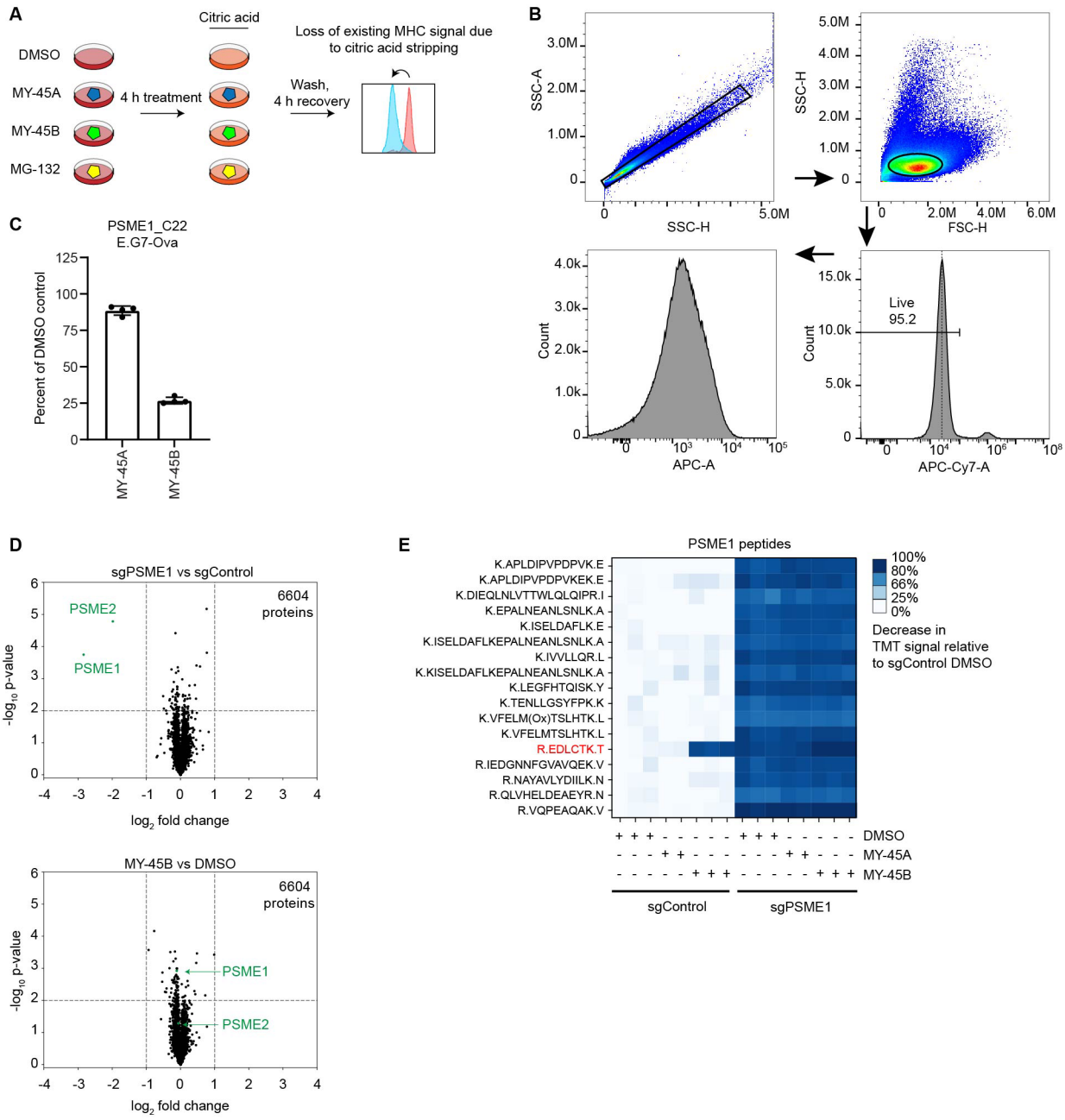

Figure S3. Chemical or genetic perturbation of PSME1 modulates MHC-I-immunopeptide interactions, related to **Figures 3** and **4**.

A. Schematic of acid wash experiment to measure recovery of MHC-I antigen presentation: Cells were treated with compound for 4 h, washed with citric acid for 2 min, then allowed to recover for up to 4 h prior to analysis by flow cytometry to measure surface presentation of SIINFEKL antigen and MHC-I.
B. Representative flow cytometry gating strategy for SIINFEKL (APC) signal quantification.
C. Quantification of PSME1_C22 engagement measured by cysteine-directed ABPP experiments performed in E.G7-Ova cells (5 μM compound, 3 h). Data are average values ± SD relative to DMSO from n = 4 independent experiments.

D. Volcano plots showing substantially (> two-fold increase or decrease) and significantly (*p* value < 0.01) changing proteins in MS-based proteomic experiments of sgPSME1 vs sgControl (sgAAVS1) cells (left) or sgControl cells treated with DMSO vs MY-45B (10 μM, 8 h). Data are average values from n = 3 independent experiments.
E. Quantification of tryptic peptides from PSME1 in MS-based proteomic experiments of sgControl and sgPSME1 cells treated with the indicated compounds (10 μM, 8 h). Note that the tryptic peptide containing PSME1_is near-completely absent in cells treated with MY-45B, but unchanged in cells treated with MY-45A or DMSO. Data are individual values relative to DMSO (n = 2-3 per group).

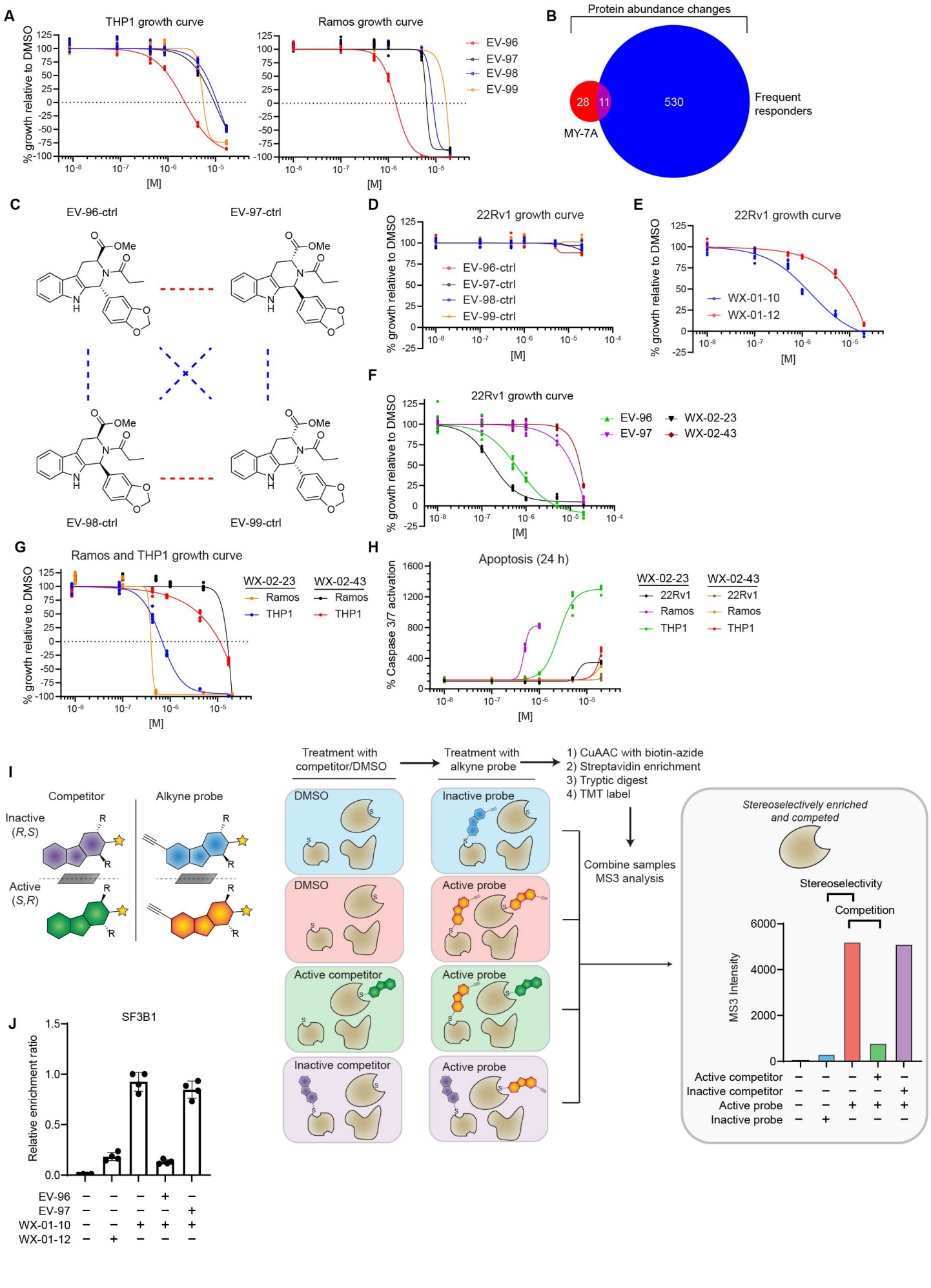
A
THP1 growth curve
Ramos growth curve
% growth relative to DMSO
[M]
EV-96
EV-97
EV-98
EV-99
B
Protein abundance changes
28
11
530
MY-7A
Frequent responders
C
EV-96-ctrl
EV-97-ctrl
EV-98-ctrl
EV-99-ctrl
D
22Rv1 growth curve
EV-96-ctrl
EV-97-ctrl
EV-98-ctrl
EV-99-ctrl
E
22Rv1 growth curve
WX-01-10
WX-01-12
F
22Rv1 growth curve
EV-96
EV-97
WX-02-23
WX-02-43
G
Ramos and THP1 growth curve
WX-02-23
Ramos
THP1
WX-02-43
Ramos
THP1
H
Apoptosis (24 h)
% Caspase 3/7 activation
WX-02-23
22Rv1
Ramos
THP1
WX-02-43
22Rv1
Ramos
THP1
I
Competitor
Alkyne probe
Inactive (R,S)
Active (S,R)
Treatment with competitor/DMSO
Treatment with alkyne probe
1) CuAAC with biotin-azide
2) Streptavidin enrichment
3) Tryptic digest
4) TMT label
DMSO
Inactive probe
DMSO
Active probe
Active competitor
Active probe
Inactive competitor
Active probe
Combine samples MS3 analysis
Stereoselectively enriched and competed
Stereoselectivity
Competition
MS3 Intensity
Active competitor
Inactive competitor
Active probe
Inactive probe
J
SF3B1
Relative enrichment ratio
EV-96
EV-97
WX-01-10
WX-01-12

Figure S4. Tryptoline acrylamides that stereoselectively engage SF3B1 alter protein abundances and block the proliferation of cancer cells, related to **Figure 5**.

A. EV-96 stereoselectively blocks the proliferation of THP1 and Ramos cells. Cells were treated with the indicated concentrations of tryptoline acrylamides for 72 h, after which cell growth was measured by CellTiter-Glo. Data are relative to DMSO control from n = 6 independent experiments.
B. Venn diagram of proteins showing > 33% decreases in abundance in 22Rv1 cells treated with EV-96 (20 μM, 8 h; see **Figure 6A**) and proteins annotated as "frequent responders" by Rupert *et al.* Only proteins quantified in both proteomic studies were included in the Venn diagram.
C. Structures of non-electrophilic analogues of tryptoline acrylamides EV-96-ctrl (**17**), EV-97-ctrl (**18**), EV-98-ctrl (**19**), and EV-99-ctrl (**20**).
D. Non-electrophilic analogues do not affect the proliferation of 22Rv1 cells. Cells were treated with the indicated concentrations of compounds for 72 h, after which cell growth was measured by CellTiter-Glo. Data are relative to DMSO control from n = 6 independent experiments.
E. Alkyne probe WX-01-10 stereoselectively blocks the proliferation of 22Rv1 cells. Cells treated with the indicated concentrations of WX-01-10 or WX-01-12 for 72 h, after which cell growth was measured by CellTiter-Glo, Data are average values ± SD relative to DMSO from n = 6 independent experiments.
F. Enhanced anti-proliferative activity of WX-02-23 compared to EV-96. 22Rv1 cells were treated with the indicated concentrations of tryptoline acrylamides for 72 h, after which cell growth was measured by CellTiter-Glo. Data are relative to DMSO control from n = 6 independent experiments.
G. Anti-proliferative activity of WX-02-23 in THP1 and Ramos cells. Cells were treated with the indicated concentrations of tryptoline acrylamides for 72 h, after which cell growth was measured by CellTiter-Glo. Data are relative to DMSO control from n = 6 independent experiments.
H. Apoptotic activity of WX-02-23 in human cancer cell lines. The indicated cell lines were treated with the indicated concentrations of tryptoline acrylamides for 24 h, after which apoptosis was measured by Caspase-Glo 3/7. Data are relative to DMSO control from n = 6 independent experiments.
I. Schematic for target identification strategy using alkyne probe enrichment and blockade of this enrichment by competitor compounds. 22Rv1 cells were treated with DMSO or active and inactive enantiomeric tryptoline acrylamides ("competitors"; 5 μM, 2 h), followed by DMSO or active and inactive enantiomeric alkyne probes (10 μM, 1 h). Cells were then harvested, lysed, and probe-labeled proteins biotinylated by CuAAC with biotin-azide, enriched with streptavidin, and analyzed by quantitative chemical proteomics. On the right, is a mock quantification profile for a candidate target responsible for stereoselective anti-proliferative activity, where such a target would show stereoselective enrichment by active alkyne probe and stereoselective blockade of this enrichment by active competitor.
J. Quantification of stereoselective enrichment and competition of SF3B1 by active alkyne probe (WX-01-10) and competitor (EV-96) vs inactive alkyne enantiomer probe (WX-01-12) and inactive enantiomer competitor (WX-02-43). Data are average values ± SD normalized to WX-01-10 treatment group for n = 4 independent experiments.

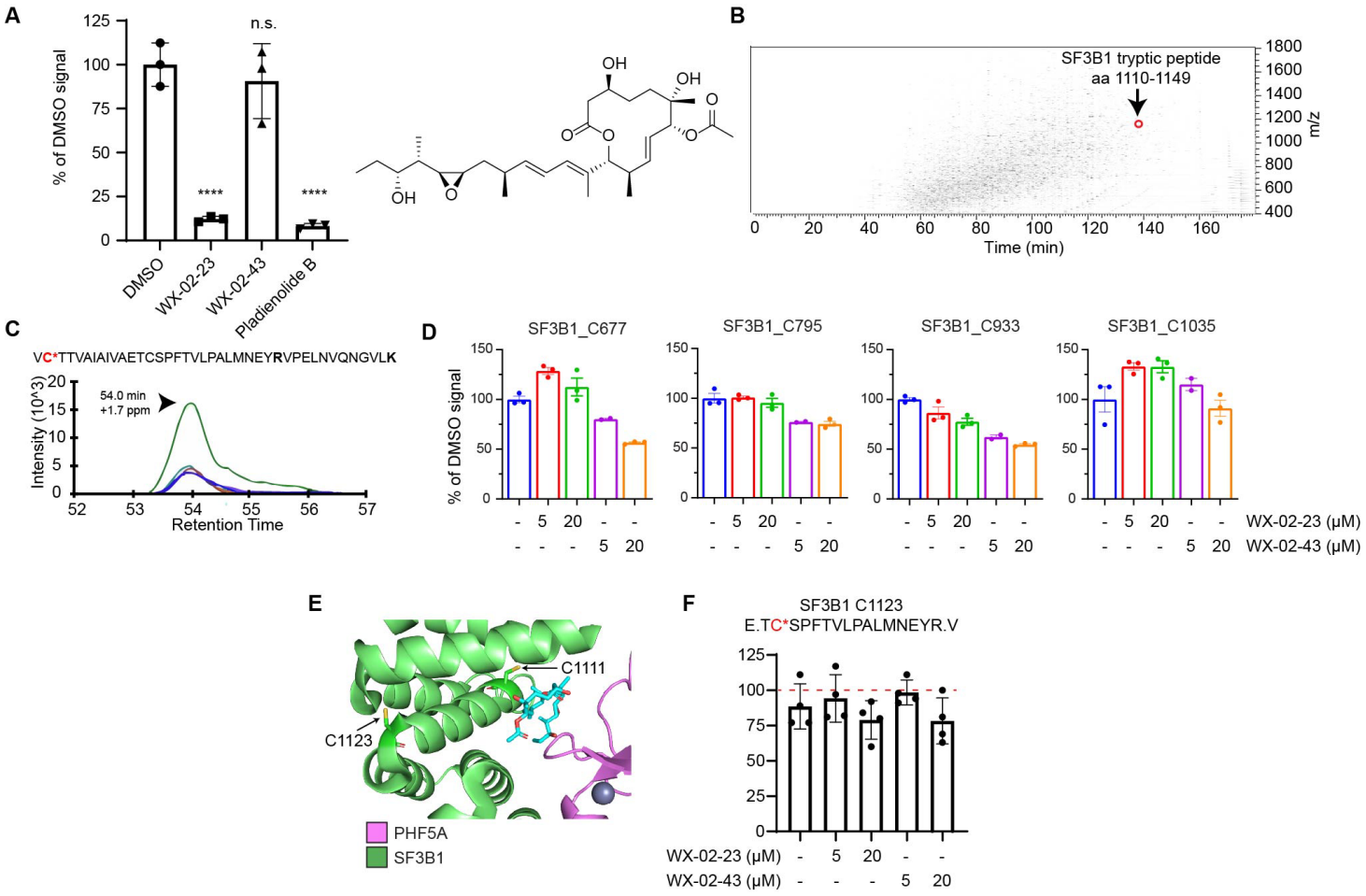

Figure S5. Tryptoline acrylamides engage C1111 of SF3B1, related to **Figure 6**.

A. Quantification of fluorescent gel data showing WX-01-10 labelling of a 150 kDa protein consistent with SF3B1, as shown in **Figure 6A**. Data are average values ± SD relative to DMSO from n = 3 independent experiments. ****, p<0.0001, Significance determined by one-way ANOVA with Dunnett's multiple comparisons test.

B. LC chromatogram of IA-DTB-labeled SF3B1 peptide (aa 1110-1149) eluting late in the gradient at ~38% acetonitrile.

C. Representative chromatogram elution profile of fragment ions for SF3B1 peptide aa 1110-1149 harboring C1111 (labeled in red).

D. Quantification of additional SF3B1 cysteines by targeted cysteine-directed ABPP, revealing that none of these residues are engaged by WX-02-23 (5 or 20 μM, 3 h) in 22Rv1 cells. Data are average values ± SD relative to DMSO from n = 2-3 independent experiments.

E. Crystal structure of SF3B1-PHF5A complex bound to pladienolide B (PDB: 6EN4), highlighting the locations of C1111 and C1123, two cysteines that are on the WX-02-23-sensitive tryptic peptide quantified by targeted cysteine-directed ABPP.

F. C1123 is not engaged by WX-02-23. Quantification of SF3B1_C1123 by cysteine-directed ABPP following trypsin and GluC digestion of proteomes from 22Rv1 cells treated with WX-02-23 or WX-02-43 (5 or 20 μM, 3 h). Data are average values ± SD relative to DMSO from n = 4 independent experiments.

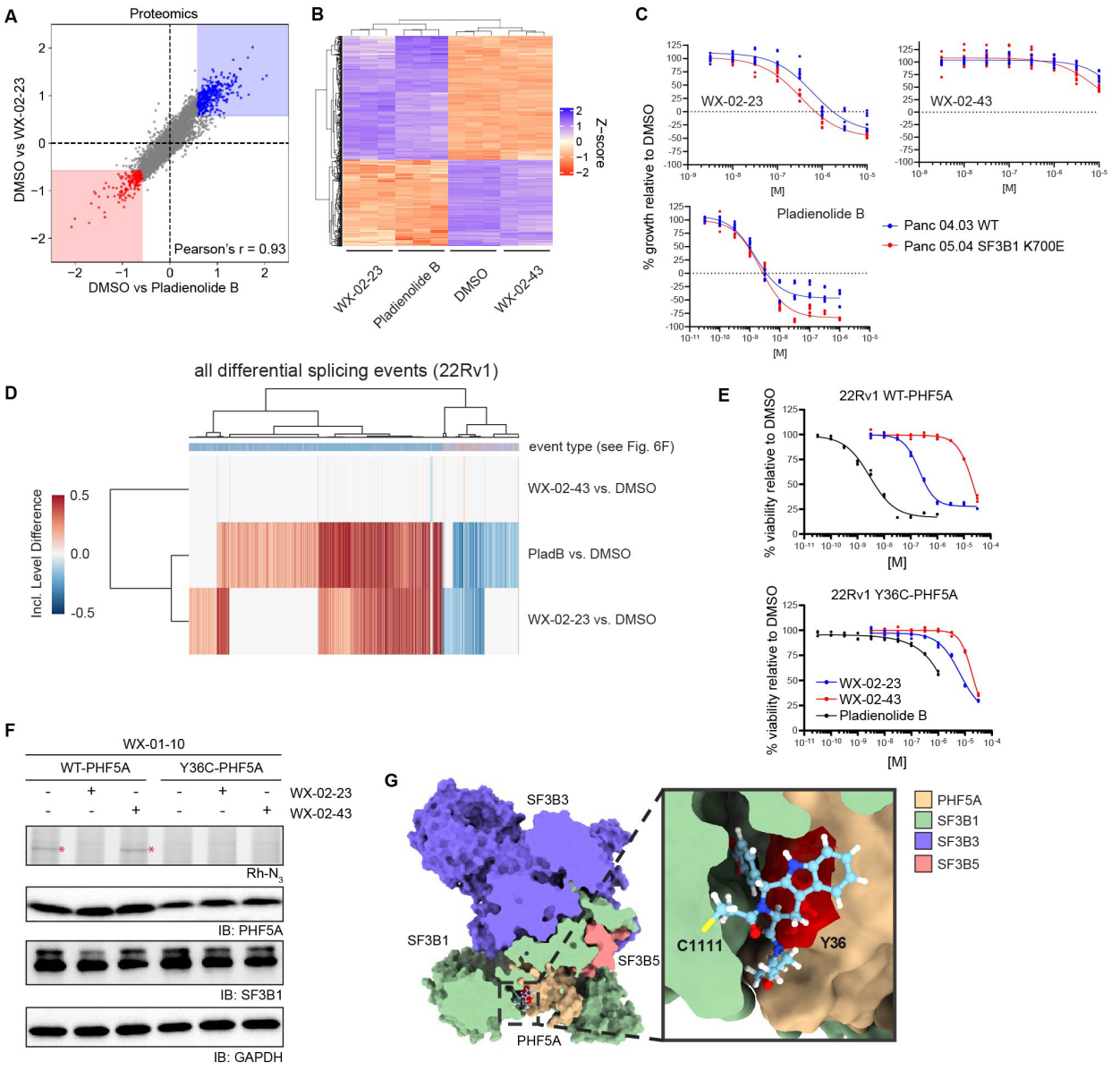

Figure S6. Tryptoline acrylamides engaging SF3B1 stereoselectively modulate spliceosome function, related to **Figure 6**.

A. Scatter plot of protein abundance changes in 22Rv1 cells treated with WX-02-23 (1 μM) pladienolide B (10 nM), or DMSO for 24 h. Proteomics data are average values shown as $\log_2$ fold change relative to DMSO for n = 4 independent experiments.

B. Hierarchical clustering of RNA-seq data showing similar changes in 22Rv1 cells treated with pladienolide B (10 nM, 8 h) or WX-02-23 (5 μM, 8 h) compared to WX-02-43 (5 μM 8 h) or DMSO-treated cells. Data are average values for n = 3 independent experiments.

C. Cell growth effects of SF3B1 ligands WX-02-23 and pladienolide B (and control compound WX-02-43) on Panc 04.03 and Panc 05.04 cells, which express WT-SF3B1 and the cancer-related K700E-SF3B1 mutant, respectively. Cells were treated with the indicated concentrations of compounds for 72 h, after which cell growth was measured by CellTiter-Glo. Data are relative to DMSO control from n = 9 independent experiments.

D. Clustered heatmap of inclusion level differences between 22Rv1 cells treated with the indicated compounds vs DMSO for all alternative splicing events from **Figure 6F**. Columns are annotated by the type of alternative splicing event in the color scheme of **Figure 6F**.
E. Cell growth effects of WX-02-23 and pladienolide B in 22Rv1 cells recombinantly expressing WT-PHF5A (upper plot) or a Y36C-PHF5A mutant (lower plot). Cells were treated with the indicated concentrations of compounds for 72 h, after which cell growth was measured by CellTiter-Glo. Data are relative to DMSO control from n = 3 independent experiments.
F. Assessment of reactivity of the WX-01-10 alkyne probe with SF3B1 in 22Rv1 cells expressing WT-PHF5A or Y36C-PHF5A by gel-ABPP. Top panel, gel-ABPP showing proteins labeled by WX-01-10 alkyne probe in the indicated cells. Cells were pre-treated with DMSO, WX-02-23 (1 μM) or WX-02-43 (1 μM) for 2 h followed by treatment with WX-01-10 (1 μM, 1 h), lysis, CuAAC with tetramethylrhodamine (TAMRA) azide, SDS-PAGE, and in-gel fluorescence scanning. Red asterisk marks a 150 kDa protein interpreted to be SF3B1 that is labeled by WX-01-10 and blocked in labeling by WX-02-23, but not inactive enantiomer WX-02-43. The labeling of SF3B1 by WX-01-10 is blocked in cells expressing the Y36C-PHF5A cells. Remaining panels represent western blots as loading controls. Results are from a single experiment representative of two independent experiments.
G. Y36 of PHF5A is located in the predicted WX-02-23 binding cavity at the interface with SF3B1. Computational predictions of small-molecule binding to SF3B1 were performed on Schrodinger Maestro (V 12.3.012, MMshare V 4.9.012, Release 2020-1, Platform Windows-x64) using a structure of pladienolide B bound to SF3B1 (PDB: 6EN4). Covalent docking was performed using Glide. Images were generated using UCSF ChimeraX [2].

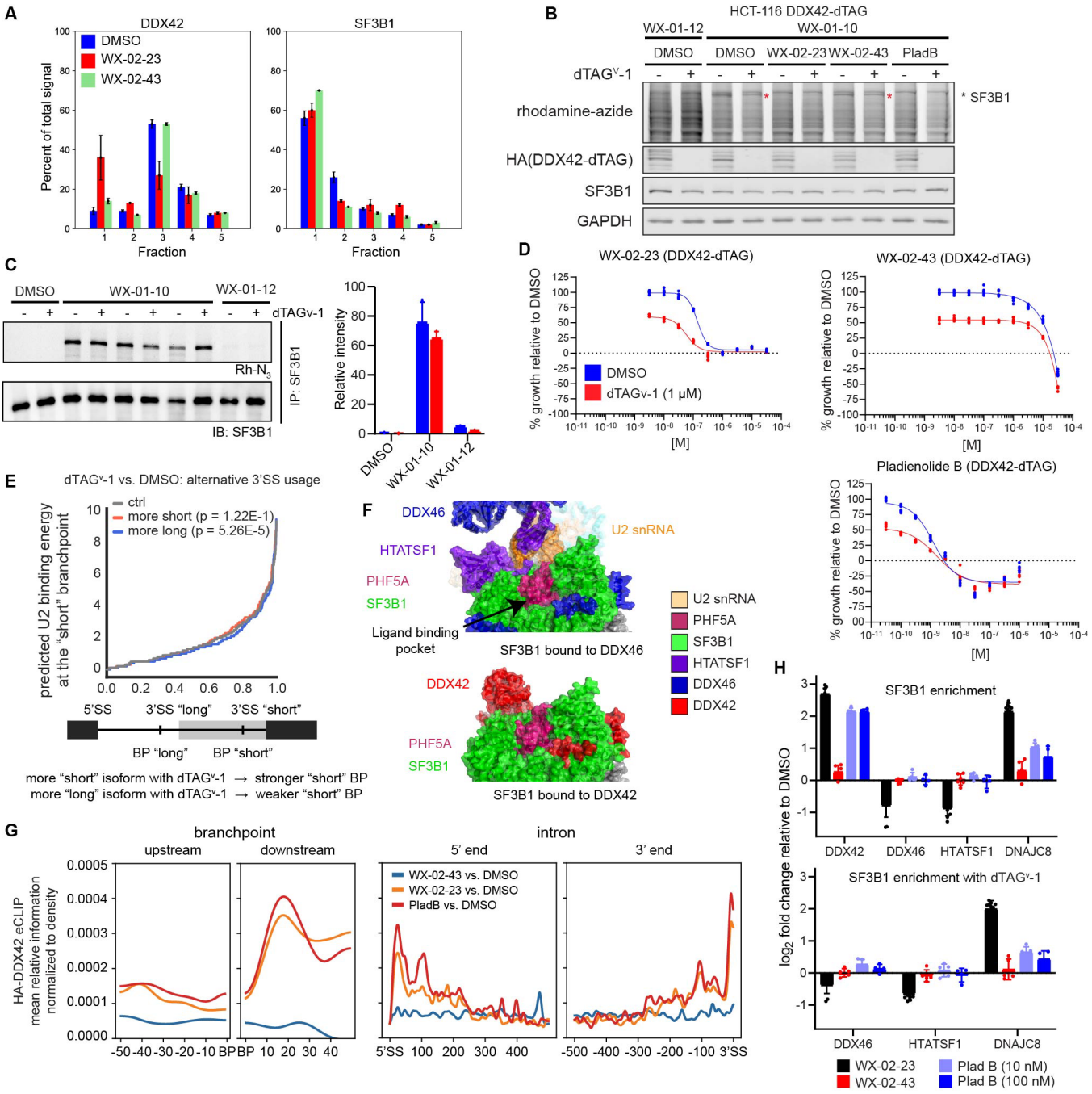

Figure S7. DDX42 facilitates branch point selection and associates more strongly with SF3B1 in WX-02-23 or pladienolide B-treated cells, related to **Figure 7**.

A. SEC-MS elution profiles for DDX42 and SF3B1 in 22Rv1 cells treated with DMSO, WX-02-23, or WX-02-43 (20 μM, 3 h). Data are average values ± SEM of the fractional distribution of reporter ion intensities from n = 2-11 independent experiments.

B. Impact of DDX42-dTAG pre-degradation on SF3B1 engagement by WX-01-10 alkyne probe as determined by gel-ABPP. DDX42-dTAG HCT-116 cells were pre-treated with dTAGv-1 (500 nM) or DMSO for 1 h and then treated with the DMSO, WX-02-23 (1 μM), WX-02-43 (1 μM), or pladienolide B (10 nM) for 2 h, followed by treatment with WX-01-10 or WX-01-12 (1 μM, 1 h) and processing for gel-ABPP as described in **Figure S6F**.

Asterisk labels the 150 kDa band interpreted as SF3B1. Results are from a single experiment representative of two independent experiments.

C. Impact of DDX42-dTAG pre-degradation on SF3B1 engagement by WX-01-10 alkyne probe as determined by gel-ABPP following immunoprecipitation of SF3B1. DDX42-dTAG HCT-116 cells were pre-treated with dTAGv-1 (500 nM) or DMSO for 1 h and then treated with WX-01-10 or WX-01-12 (2.5 μM) for 1 h. Immunoprecipitation was performed with an anti-SF3B1 antibody (CST #14434) followed by CuAAC of immunprecipitated proteins to a tetramethylrhodamine-azide- tag and analysis by SDS-PAGE and in-gel fluorescence scanning (top image) or western blotting (bottom image). Quantification normalized to SF3B1 enrichment from gel (left) is shown (right).

D. Growth effects of WX-02-23 or pladienolide B in cells lacking DDX42. DDX42-dTAG HCT-116 cells were pre-treated with dTAGv-1 (1 μM) or DMSO for 1 h and then treated with the indicated concentrations of WX-02-23, pladienolide B (PladB), or the control compound WX-02-43 for 72 h, after which cell growth was measured by CellTiter-Glo. Data are relative to DMSO control from n = 6 independent experiments.

E. DDX42 loss increased the usage of stronger branch point sequences and decreased the usage of weaker branch points at differentially included exons BP usage. DDX42-dTAG HCT-116 cells were pre-treated for 1 h with either 500 nM dTAGv-1 or DMSO, followed by addition of either DMSO or compounds to the same supernatant for 8 h. Data are from the union of n = 3 biological replicates.

F. Cryo-EM structures of SF3B1 bound to DDX46/HTATSF1 (PDB: 7EVO) or DDX42 (PDB: 7EVN). Structures were overlayed and the same perspective is shown demonstrating the shared interaction sites of DDX42 and DDX46/HTATSF1 with SF3B1.

G. Effects of SF3B1 ligands WX-02-23 and pladienolide B (PladB) on metadensity plots of HA-DDX42 eCLIP signal (relative information of IP of indicated treatment over IP of DMSO). DDX42-dTAG HCT-116 cells were treated with WX-02-23 (5 μM), WX-02-43 (5 μM), or pladienolide B (100 nM) for 3 h after which DDX42 eCLIP experiments were performed using the HA-tag of the dTAG fusion. Data are average values from the union of n = 2 independent experiments.

H. Quantification of proteins showing differential co-immunoprecipitation with SF3B1 in cells treated with WX-02-23 or pladienolide B (PladB) and the effect of DDX42 disruption on these interactions. Cells were pre-treated with dTAGv-1 (500 nM) or DMSO for 1 h and then treated with WX-02-23 (5 μM), WX-02-43 (5 μM), pladienolide B (100 nM), or DMSO for 3 h. Co-immunoprecipitation analysis was performed with anti-SF3B1 antibody (CST #14434) followed by MS-based proteomics. Note that pladienolide B was maintained in the lysis and immunoprecipitation buffers to preserve its effect on SF3B1 interacting proteins throughout the co-immunoprecipitation process. Data are average values ± SD relative to DMSO from n = 4-10 independent experiments.

REFERENCES

1. Kirkwood, K.J., Ahmad, Y., Larance, M., and Lamond, A.I. (2013). Characterization of Native Protein Complexes and Protein Isoform Variation Using Size-fractionation-based Quantitative Proteomics. Molecular & Cellular Proteomics : MCP *12*, 3851-3873. 10.1074/mcp.M113.032367.
2. Pettersen, E.F., Goddard, T.D., Huang, C.C., Meng, E.C., Couch, G.S., Croll, T.I., Morris, J.H., and Ferrin, T.E. (2021). UCSF ChimeraX: Structure visualization for researchers, educators, and developers. Protein Sci *30*, 70-82. 10.1002/pro.3943.